

This discussion paper is/has been under review for the journal Biogeosciences (BG).
Please refer to the corresponding final paper in BG if available.

A latitudinally-banded phytoplankton response to 21st century climate change in the Southern Ocean across the CMIP5 model suite

S. Leung^{1,2}, A. Cabré², and I. Marinov²

¹School of Oceanography, University of Washington, Seattle, WA, USA

²Department of Earth and Environmental Science, University of Pennsylvania, Philadelphia, PA, USA

Received: 26 April 2015 – Accepted: 28 April 2015 – Published: 2 June 2015

Correspondence to: S. Leung (shirlleu@uw.edu)

Published by Copernicus Publications on behalf of the European Geosciences Union.

BGD

12, 8157–8197, 2015

A
latitudinally-banded
phytoplankton
response

S. Leung et al.

Title Page

Abstract

Introduction

Conclusions

References

Tables

Figures

⏪

⏩

◀

▶

Back

Close

Full Screen / Esc

Printer-friendly Version

Interactive Discussion



Abstract

Changes in Southern Ocean (SO) phytoplankton distributions with future warming have the potential to significantly alter nutrient and carbon cycles as well as higher trophic level productivity both locally and throughout the global ocean. Here we investigate the response of SO phytoplankton productivity and biomass to 21st century climate change across the CMIP5 Earth System Model suite. The models predict a zonally-banded pattern of phytoplankton abundance and production changes within 4 regions: the subtropical ($\sim 30^\circ$ S to 40° S), transitional ($\sim 40^\circ$ S to 50° S), subpolar ($\sim 50^\circ$ S to 65° S) and Antarctic (south of $\sim 65^\circ$ S) bands. We find that shifts in bottom-up variables (nitrate, iron, and light availability) drive changes in phytoplankton abundance and production on not only interannual, but also decadal and 100-year timescales: the timescales most relevant to climate change. Spatial patterns in the modeled mechanisms driving these biomass trends qualitatively agree with recent observations, though longer-term records are needed to separate the effects of climate change from those of interannual variability. Because much past observational work has focused on understanding the effects of the Southern Annular Mode (SAM) on biology, future work should attempt to quantify the precise influence of an increasingly positive SAM on SO biology within the CMIP5 models. Continued long-term in-situ and satellite measurements of SO biology are clearly needed to confirm model findings.

1 Introduction

The photosynthetic activity of marine phytoplankton provides the ultimate source of food for virtually all marine biota, including organisms of vast commercial value. This phytoplanktonic activity also drives the biological pump, the process by which surface carbon dioxide and nutrients are drawn down via photosynthesis with subsequent sinking of organic matter to the deep ocean that effectively removes carbon from the atmosphere for centuries to millennia (Eppley and Peterson, 1979; Heinze et al., 1991).

A latitudinally-banded phytoplankton response

S. Leung et al.

Title Page

Abstract

Introduction

Conclusions

References

Tables

Figures



Back

Close

Full Screen / Esc

Printer-friendly Version

Interactive Discussion



A latitudinally-banded phytoplankton response

S. Leung et al.

Title Page

Abstract

Introduction

Conclusions

References

Tables

Figures

◀

▶

◀

▶

Back

Close

Full Screen / Esc

Printer-friendly Version

Interactive Discussion



The warming trend recorded in the global surface ocean since the mid-20th century is projected to continue in the 21st century (Stocker et al., 2013) and can impact phytoplankton activity both directly via the physiological effect of temperature on growth rate and/or indirectly by altering key environmental factors such as nutrient and light availability (e.g., Marinov et al., 2010). The responses of phytoplankton communities to climate change may have profound ecological and biogeochemical repercussions with potential feedbacks on climate, the net sign and magnitude of which are still largely uncertain. Documenting and understanding these responses is one of the main goals of global change science today (Falkowski et al., 2000; Geider et al., 2001).

As a major region of deep, intermediate, and mode water formation, the Southern Ocean (SO) is one of the few places on earth where there is direct communication between the atmosphere and the deep ocean. Because of this, the SO plays a critical role in the global climate system via its significant impacts on the global heat and carbon budgets. Additionally, intermediate and mode waters formed here allow for large advective transfers of macronutrients such as nitrate, phosphate, and silicate from the SO to the low-latitude oceans, indirectly accounting for up to 75% of phytoplankton production north of 30° S (Sarmiento et al., 2004a; Marinov et al., 2006). Thus, potential changes in SO productivity can affect not only local nutrient and carbon cycles, but may also drastically alter nutrient and carbon cycles as well as phytoplankton distributions throughout the global ocean.

Much of the SO is a so-called HNLC (high-nutrient, low-chlorophyll) region, where chlorophyll concentrations (and implicitly phytoplankton biomass and production) are relatively low, in spite of a large upwelled supply of macronutrients (e.g., Martin et al., 1990; Cullen, 1991; Pitchford and Brindley, 1999). Here insufficient light availability may help explain why biological productivity is not as high as it could be. Because light is a potentially stronger limiting factor than macronutrient supply for photosynthesis here, warming is generally postulated to be advantageous for algal communities within these regions because shallower mixed layer depths (MLDs) (due to enhanced stratification and increased freshwater influx with future warming) are expected to increase light

availability to phytoplankton and prolong the growing season (Bopp et al., 2001; Le Quéré et al., 2005; Doney, 2006). Warming may also directly enhance productivity by alleviating growth rate limitations due to low temperatures (Steinacher et al., 2010). If this line of reasoning holds, we should observe an increase in phytoplankton biomass and chlorophyll concentrations in the high-latitude SO with future warming. A further complicating factor, however, is that SO phytoplankton are also limited by iron and silicate, such that they can be light-iron-silicate (or any combination of the three) co-limited (Moore et al., 2013). Thus, changes in any of these factors will affect phytoplankton productivity and biomass within the SO. Because of the complicated multifactor nature of the problem, a synergy of observations and models is needed to understand the driving mechanisms of projected changes in SO phytoplankton distributions.

Recent studies have suggested that SO phytoplankton biomass and productivity will change in response to rising atmospheric CO₂ concentrations, but the direction, significance, and causes of these changes are still under debate (Bopp et al., 2001, 2005; Schmittner et al., 2008; Steinacher et al., 2010; Wang and Moore, 2012; Bopp et al., 2013; Marinov et al., 2013; Cabré et al., 2014; Laufkötter et al., 2015). Here we use the newest generation of fully-coupled CMIP5 (Coupled Model Intercomparison Project 5) Earth System Models to systematically study the response of SO phytoplankton to 21st century climate change, assuming the *rcp8.5* emissions scenario. All 16 of the CMIP5 models that incorporate ecological subroutines and provide their output on the CMIP5 portal are included in our study. We also summarize and review past field studies of SO phytoplankton to see what has already been observed and to understand where there may be disagreement over mechanisms and/or recent directions of changes. We find that over the next 100-years, the CMIP5 models predict a *zonally-banded pattern* of SO phytoplankton abundance and productivity changes driven by shifts in light, nitrate, and iron availability with future warming. We show that the SO south of ~30° S can be separated into 4 zonally-defined biomes: the subtropical (30° S to 40° S), transitional (~40° S to 50° S), subpolar (~50° S to 65° S) and Antarctic (south of ~65° S) bands. Each of these biomes shows consistent ecological responses to 21st century

BGD

12, 8157–8197, 2015

A
latitudinally-banded
phytoplankton
response

S. Leung et al.

Title Page

Abstract

Introduction

Conclusions

References

Tables

Figures

◀

▶

◀

▶

Back

Close

Full Screen / Esc

Printer-friendly Version

Interactive Discussion



climate change across most of the CMIP5 models studied. We further find that this banded structure is in general qualitative agreement with patterns and mechanisms of phytoplankton distribution changes which have emerged from observations over recent decades.

2 Methods

2.1 CMIP5 models and scenarios

A list of the models used along with relevant model details are listed in Table 1. The scenarios used in our study are the *historical* and *rcp8.5* scenarios from the IPCC's Fifth Assessment Report, with output data downloaded from http://cmip-pcmdi.llnl.gov/cmip5/data_portal.html. Only the first ensemble members (r1ip1) within the archives are used here. The *historical* scenario, spanning years 1850–2005, is forced with observed atmospheric CO₂ concentrations and is used to represent present-day conditions. The *rcp8.5* scenario, spanning years 2006–2100, is representative of future unmitigated climate change conditions with radiative forcing increasing by 8.5 W m⁻² relative to preindustrial by year 2100. See Taylor et al. (2012) and van Vuuren et al. (2011) for further details on CMIP5 experimental design and forcing scenarios.

2.2 Absolute and relative 100-year mean changes

Absolute 100-year mean changes are calculated as the mean value from years 1980–1999 within the *historical* simulation subtracted from the mean value from years 2080–2099 within the *rcp8.5* simulation. Relative change is defined as the 100-year absolute change divided by the *historical* 1980–1999 mean.

BGD

12, 8157–8197, 2015

A latitudinally-banded phytoplankton response

S. Leung et al.

Title Page

Abstract

Introduction

Conclusions

References

Tables

Figures

◀

▶

◀

▶

Back

Close

Full Screen / Esc

Printer-friendly Version

Interactive Discussion



2.3 Model weights

We weight models based on their similarity in order to avoid double counting and to preserve model independence. If two models are very similar in terms of their ocean biogeochemistry or physics (typically because they are two slightly different versions of the same basic model coming from the same modeling center – see Fig. S1 comparing phytoplankton biomass changes in HadGEM2-CC and HadGEM2-ES, for example), we give them each a weight of 0.5 instead of 1. See Table 1 for a list of model weights and Cabré et al. (2014) for a more detailed discussion on weighting. We do not attempt to weight models according to how well they reproduce observed chlorophyll *a* (chl) concentrations or primary productivities for the following reasons: (1) We cannot tell if they reproduce current mean-state values of these variables for the right reasons, and (2) we would like to understand equally the reasons for each individual CMIP5 model's predictions and the reasons for the entire suite's predictions on average.

2.4 Bootstrap analysis (Figs. 1 and 5, S16)

In order to quantify the percentage of simulated model realizations that agree on the sign of a predicted trend, we use the statistical technique known as bootstrapping. Here each realization is the weighted average over n models (where n is the number of models with data available for any given variable) that are selected randomly with replacement among the n available models. In this way, one model may be represented more than once, while other models may not be represented at all within a single realization. We take into account interannual variability by randomly selecting one of the 20 years from the present-day *historical* scenario (1980–1999) and one from the future *rcp8.5* climate change scenario (2080–2099) for each randomly selected model in each realization. For every variable of interest at every grid point, we create 1000 realizations of the 100-year trend by finding the difference between the two randomly chosen years. We then obtain the multi-model significance of this trend at each grid

BGD

12, 8157–8197, 2015

A latitudinally-banded phytoplankton response

S. Leung et al.

Title Page

Abstract

Introduction

Conclusions

References

Tables

Figures

◀

▶

◀

▶

Back

Close

Full Screen / Esc

Printer-friendly Version

Interactive Discussion



second of all, we would like to tease out the dominant driver of the net phytoplankton response within the zonal band of interest and masking helps to further amplify the signal we are looking for by focusing on what the majority of points we are interested in are doing, thus effectively diluting the confounding effects of natural background variability.

To confirm that masking does not significantly alter our results besides by potentially enhancing the signal-to-noise ratio of our correlations, we repeat our analyses (namely, Figs. 2–4) using all (both masked and unmasked) grid points. Results from these all-inclusive analyses agree with those presented here for masked points only, but with slightly weaker correlation coefficients between phytoplankton biomass or productivity and a given driving variable of interest, as expected (Figs. S13, S15).

2.6 Creating control and climate change time series (Fig. 2)

In order to remove the effects of climate change and create a *control* time series reflecting interannual variations alone, we detrended raw yearly time series data (*historical* from 1911–2005, *rcp8.5* from 2006–2100) by subtracting a 25-year running mean from each yearly data point. To create a second time series retaining variability on a longer than interannual but shorter than decadal timescale, we took the 5-year running mean of the raw yearly time series data and then subtracted a 25-year running mean from each 5-year running mean-smoothed annual value. Finally, in order to investigate and emphasize the effects of climate change, we created a *climate change* time series by taking 10-year averages (not running means, but rather averages of non-overlapping 10-year intervals) of the same raw yearly time series data as before.

2.7 Attainment and processing of observational and reanalysis data (Fig. 6)

Monthly ocean temperature and salinity reanalysis products from the Met Office Hadley Centre's EN3 dataset (<http://www.metoffice.gov.uk/hadobs/en3/>) were used to calculate summertime MLD anomalies from 1950–2013. Synoptic monthly mean reanalysis products of total cloud cover from December 1980–February 2013

BGD

12, 8157–8197, 2015

A latitudinally-banded phytoplankton response

S. Leung et al.

Title Page

Abstract

Introduction

Conclusions

References

Tables

Figures

⏪

⏩

◀

▶

Back

Close

Full Screen / Esc

Printer-friendly Version

Interactive Discussion



were downloaded from the ERA-INTERIM dataset (<http://www.ecmwf.int/en/forecasts/datasets/era-interim-dataset-january-1979-present>) and then averaged over the summer months (December to February) to generate a time series of yearly summertime average total cloud cover. Monthly satellite chl anomalies calculated with the latest version of the SeaWiFs band-ratio algorithm (OC4v6) were obtained from the SeaWiFS dataset (<http://oceancolor.gsfc.nasa.gov/cgi/l3>) for the months September 1997–December 2010. All trends are expressed as the slope of a least-squares best-fit line to the given time series at each grid point. Statistical significance of trends was determined using a two-tailed t test at the 5 % significance level. In addition to analysis of these aforementioned datasets, we also compile an extensive array of past SO biogeochemical observations and summarize those results.

3 Results and discussion

3.1 Zonally-banded all-model mean 100-year changes

In order to study predicted phytoplankton responses to climate change in the SO, we focus on 100-year changes in the maximum annual surface phytoplankton biomass (henceforth PB, representative of phytoplankton biomass at the peak of an annual bloom) and primary production annually averaged and vertically integrated down to 100 m depth (henceforth PP). Whenever we analyze individual models, we use PB because we frequently only have monthly model output at the surface of the ocean (i.e., monthly NO_3 , iron, and light output are only available at the surface) and want to keep the variables we are cross-correlating consistent whenever possible (either all variables at the surface only or all vertically-integrated only). Furthermore, PB is more directly comparable to surface satellite observations of phytoplankton (see Sect. 3.4). Although PB and PP are obviously different biological quantities (PB is surface phytoplankton biomass concentration and is directly affected by grazing, while PP is the integrated product of growth rate and biomass and is only indirectly affected by grazing

BGD

12, 8157–8197, 2015

A latitudinally-banded phytoplankton response

S. Leung et al.

Title Page

Abstract

Introduction

Conclusions

References

Tables

Figures

◀

▶

◀

▶

Back

Close

Full Screen / Esc

Printer-friendly Version

Interactive Discussion



– see references cited in Table 1 for model equation details), the direction of projected changes in the two variables are highly similar in our regions of interest (Fig. 1a and b; Figs. S1–2). Some exceptions to this occur between ~ 50 – 65° S in models GISS-E2-H-CC and CESM1-BGC (Figs. S1–2); here PP increases while PB decreases, suggesting that the effects of top-down controls (grazing) win out over the effects of bottom-up controls (nutrients, light, temperature). Among the other models as well as other regions within these two models, however, changes in bottom-up controls appear to explain most of the projected phytoplankton response such that patterns of predicted PP and PB change overlap significantly. Because of this and large uncertainties in how well the models' grazing parameterizations approximate the real ocean due to their incomplete foodweb dynamics (see references cited in Table 1 for model equation details), we focus mostly on understanding the effects of bottom-up controls within these models. One other notable difference between PB and PP is that trends in PP appear to be slightly more regionally consistent across the models than trends in PB (Figs. S1–2; Fig. S16), so that whenever we look at relationships across models, we use PP instead of PB. PP output is also available for a larger number of the models.

Predicted multi-model mean 100-year changes in both PB and PP exhibit a zonally-banded pattern similar to those predicted by individual models alone (Fig. 1a and b; Figs. S1–2; Tables S1–2). This leads to a natural division of the SO into four zonally-banded biomes separated by switches in the sign of predicted PB and PP changes, as follows:

1. Subtropical – Within the first zonal band ($\sim 30^\circ$ S to $\sim 40^\circ$ S), there is a predicted decrease in PB and PP and wintertime nitrate concentrations (Fig. 1c; Fig. S3). Here shallower wintertime MLDs (Fig. S4) and resulting decreases in nitrate supply are associated with increases in water column stratification and the climate-driven poleward expansion of subtropical gyres observed across all CMIP5 models (Meijers et al., 2012; Cabré et al., 2014).

BGD

12, 8157–8197, 2015

A
latitudinally-banded
phytoplankton
response

S. Leung et al.

Title Page

Abstract

Introduction

Conclusions

References

Tables

Figures

◀

▶

◀

▶

Back

Close

Full Screen / Esc

Printer-friendly Version

Interactive Discussion



A latitudinally-banded phytoplankton response

S. Leung et al.

Title Page

Abstract

Introduction

Conclusions

References

Tables

Figures

◀

▶

◀

▶

Back

Close

Full Screen / Esc

Printer-friendly Version

Interactive Discussion

2. Transitional – Within the second zonal band ($\sim 40^\circ$ S to $\sim 50^\circ$ S), the models predict an increase in PB and PP with climate change, which we attribute to a shoaling of the summertime MLD (which alleviates light limitation) present during the peak of phytoplankton blooms (Fig. 1d; Fig. S5), as well as an increase in wintertime iron supply associated with the deepening of wintertime MLDs (Fig. 1e; Figs. S4, S6).
3. Subpolar – Within the third zonal band ($\sim 50^\circ$ S to $\sim 65^\circ$ S), we ascribe a predicted drop in modeled PB and PP over the 21st century to deeper summertime MLDs (Fig. 1d; Fig. S5) and decreased summertime IPAR (incident photosynthetically active radiation) (Fig. 1f; Fig. S7) due to increased total cloud fraction (Fig. 1g; Fig. S8), both of which exacerbate phytoplankton light limitation in this region.
4. Antarctic – South of $\sim 65^\circ$ S, a second region of predicted PB and PP increase is associated with enhanced iron supply (Fig. 1e; Fig. S6) and increased light availability due to accelerated melting of sea ice (Fig. 1f; Fig. S7).

These abovementioned factors are proximate physical and biogeochemical drivers of predicted phytoplankton responses within the models, but what is the ultimate driver of all of these physical and biogeochemical changes? One highly agreed upon dynamical change captured within all of the models analyzed here is an intensification and poleward shift of the SO westerly wind belt (Fig. 1h; Fig. S9) associated with an increasingly positive phase of the Southern Annular Mode (SAM) with future warming (e.g., Yin, 2005; Arblaster and Meehl, 2006; Russell et al., 2006; Gillett and Fyfe, 2013; Zheng et al., 2013; see also Fig. S10 for projected SAM time series within the CMIP5 models and Sect. 3.4 for a discussion of SAM within observations). This highly consistent increase in wind stress (which is most pronounced in the summer – plots not shown) south of 50° S may explain the deepening of summertime MLDs south of 50° S, while the decrease in wind stress between 30° S and 50° S may explain the shoaling of summertime MLDs in that region (Fig. 1d; Fig. S5). These changes in MLD can then affect nutrient supply to the surface, perhaps leading to the large decreases in

nificantly correlated with PB over at least two of the three (interannual, 5-year, and decadal) studied timescales are shown (see Fig. S12 for examples of how correlations between PB and variables which were *not* chosen looked in comparison to the correlations between PB and the variable which *was* chosen). The driving variables shown in Fig. 2 are thus the ones whose relationships with PB hold on interannual, 5-year, as well as longer-term climate change timescales in both the *historical* and *rcp8.5* scenarios. Significantly, this implies that changes in these particular variables are the likely drivers of changes in phytoplankton biomass on an interannual as well as a longer-term timescale associated with future warming.

PB between 30° S and 40° S is strongly positively correlated with maximum annual surface nitrate concentration in all three models on all timescales (Fig. 2a). This suggests that predicted future decreases in PB between 30° S and 40° S are largely driven by climate warming-induced decreases in macronutrient supply to the surface during winter. This decreased supply is in turn a consequence of increased water column stratification and decreased maximum annual wintertime MLD associated with future warming, as was suggested by the analysis of multi-model mean maps discussed in Sect. 3.1 above.

Between 40° S and 50° S, projections of enhanced PB are driven by either increases in iron concentrations (GFDL-ESM2G and IPSL-CM5A-MR) or reduced light limitation associated with shoaling of the summertime mixed layer (HadGEM2-ES) (Fig. 2b), again in agreement with the analysis in Sect. 3.1.

Within the 50° S to 65° S band, where PB is predicted to decrease across all three models, light and iron are the most important limiting factors (Fig. 2c). For GFDL-ESM2G, in regions within this band where PB decreases with climate change, cloud cover (which is negatively correlated with PB – plot not shown) increases, leading to a concomitant decrease in surface light availability, which is positively correlated with PB (Fig. 2c). Furthermore, in both GFDL-ESM2G and HadGEM2-ES, the summertime MLD is predicted to deepen with climate change, creating an even more light-limited environment for phytoplankton here (Fig. 2c), as was deduced using multi-model means in

BGD

12, 8157–8197, 2015

A
latitudinally-banded
phytoplankton
response

S. Leung et al.

Title Page

Abstract

Introduction

Conclusions

References

Tables

Figures

◀

▶

◀

▶

Back

Close

Full Screen / Esc

Printer-friendly Version

Interactive Discussion



Sect. 3.1. In contrast to the first two models and missing from the analysis in Sect. 3.1, IPSL-CM5A-MR's wintertime surface iron concentrations appear to play the biggest role in determining PB between 50–65° S (wintertime MLD was also well-correlated with PB on all studied timescales here, most likely because it drives the supply of iron from the deep ocean) (Fig. 2c).

South of 65° S, iron is significantly positively correlated with PB on all three timescales within the models GFDL-ESM2G and IPSL-CM5A-MR (Fig. 2d), as was expected from multi-model mean change analyses in Sect. 3.1. For HadGEM2-ES, both average annual sea ice fraction and maximum annual IPAR were significantly correlated with PB south of 65° S, such that available light at the ocean surface is likely the limiting factor within this model's Antarctic band. An increase in IPAR due to a decrease in sea ice fraction is thus the most probable cause of projected phytoplankton abundance increases here, again in agreement with the reasoning in Sect. 3.1.

In sum, these findings from Fig. 2 agree well with those deduced from Fig. 1, as discussed in Sect. 3.1 above. In particular, within each zonally-banded biome, the proposed drivers of projected phytoplankton responses in the all-model means are the same ones driving phytoplankton responses within the individual models studied here. Results for Fig. 2 were the same but with slightly smaller correlation coefficients when using all (both masked and unmasked) grid points (see Fig. S13).

3.2.2 Centennial time-scale analysis

To confirm that the bottom-up controls on PB proposed in Sects. 3.1 and 3.2.1 hold across the four SO biomes on even longer 100-year timescales, we undertake a spatial correlation analysis within the same three models as before. In Fig. 3, we show the results of this spatial correlation analysis in which we look at the relationship between 100-year changes in PB and the variables of interest at every grid point within each masked latitudinal band. Each dot in a scatter plot represents a masked grid point which undergoes a 100-year change in a variable of interest and an associated change in PB at that same grid point. By plotting only those variables with the largest magni-

BGD

12, 8157–8197, 2015

A latitudinally-banded phytoplankton response

S. Leung et al.

Title Page

Abstract

Introduction

Conclusions

References

Tables

Figures

◀

▶

◀

▶

Back

Close

Full Screen / Esc

Printer-friendly Version

Interactive Discussion



tude correlation coefficients when correlated with PB, we are able to discover which variables affect PB most in each latitudinal band over 100-year timescales within each of the three models studied in detail (see Fig. S14 for an example of how correlations between PB and variables *not* chosen looked in comparison to correlations between PB and the variable chosen). For each chosen variable, scatter plots of either relative or absolute 100-year changes are shown, depending on which type of change generated the clearest relationship between PB and the variable of interest. As for Fig. 2, results for Fig. 3 were the same but with slightly smaller correlation coefficients when using all (both masked and unmasked) grid points (see Fig. S15).

Together, Figs. 2 and 3 show that the variables of interest within each zone that drive PB on decadal and shorter timescales also tend to be those that drive PB on an even longer 100-year climate change timescale. There are, however, a couple of important discrepancies. The first occurs in GFDL-ESM2G within the 50–65° S band, where light limitation is shown to be most important on decadal and shorter timescales (Fig. 2c) while iron limitation appears to take over on a 100-year timescale (Fig. 3c). This suggests the presence of iron-light co-limitation in this region within GFDL-ESM2G, in agreement with both theory and previous studies (e.g., Sunda and Huntsman, 1997; Boyd et al., 2001; Feng et al., 2010). The second discrepancy occurs in IPSL-CM5A-MR within the south-of-65° S band, where iron limitation is most important on decadal and shorter timescales (Fig. 2d) while increases in sea surface temperature (SST) become the dominant driver of PB increases on a 100-year timescale (Fig. 3d) (though iron is still somewhat important on the centennial timescale with $R = 0.703$ when spatially correlated with PB change – plot not shown).

In sum, we find that for the most part, the mechanisms within each zonal band that determine PB on decadal and shorter timescales tend to be those that determine PB on longer, centennial climate change-driven timescales as well. The magnitude of each driver's effect on phytoplankton biomass (as seen from the slopes of best-fit lines in Figs. 2–3) also remains the same across the relevant timescales, further supporting the notion that the same mechanisms act on the different timescales studied.

BGD

12, 8157–8197, 2015

A latitudinally-banded phytoplankton response

S. Leung et al.

Title Page

Abstract

Introduction

Conclusions

References

Tables

Figures

◀

▶

◀

▶

Back

Close

Full Screen / Esc

Printer-friendly Version

Interactive Discussion



3.3 Consistency of trends and mechanisms driving phytoplankton changes across all models

3.3.1 Drivers of 100-year phytoplankton changes across all models

Finally, we ask whether the mechanisms proposed in Sects. 3.1 and 3.2 above hold across all 16 CMIP5 models with explicit phytoplankton biology. To answer this, we plot 100-year changes in PP vs. 100-year changes in the variables of interest across all of the models and look for among-model agreement as to the effect of these variables on PP within each masked zonal band (Fig. 4). Here we only box and highlight the points driven by mechanisms which could be logically predicted from theory or model equations. For example, although almost all models undergo increases in cloud fraction and primary production south of 65° S, we do not box the orange points in the PP vs. average annual cloud cover plot (Fig. 4e) because we know from both accepted theory and model equations that an increase in cloud fraction would decrease light availability and consequently lead to decreases, not increases, in primary production. Thus, we can safely ignore changes in cloud cover as a driver of changes in primary production among the models south of 65° S and instead view these changes in cloud cover as merely a consequence of underlying dynamical changes occurring in that region already. Via this technique, we find a consistent set of mechanisms driving 100-year changes in productivity across the CMIP5 model suite (highlighted by colored boxes in Fig. 4), in agreement with the mechanisms brought to light by the analyses in Sects. 3.1 and 3.2.

Nitrate emerges as the driver for changes in PP within the 30–40° S band across all models (i.e., all red points lie in the third quadrant and within the red box in Fig. 3b). Models with greater relative decreases in wintertime surface nitrate concentrations undergo significantly ($p < 0.05$) greater decreases in average production within the 30–40° S band. Within the 40–50° S band, models with increases in relative iron concentration and decreases in summertime MLD also experience relative increases in PP (Fig. 3a and c, purple boxes). Further solidifying the importance of climate-driven

BGD

12, 8157–8197, 2015

A latitudinally-banded phytoplankton response

S. Leung et al.

Title Page

Abstract

Introduction

Conclusions

References

Tables

Figures

⏪

⏩

◀

▶

Back

Close

Full Screen / Esc

Printer-friendly Version

Interactive Discussion



changes in light availability (in turn driven by summertime MLD, cloud fraction, and IPAR) within the 50–65° S band, models predicting relative increases in summertime MLD or average annual cloud cover, along with decreases in maximum annual IPAR, also predict relative decreases in PP in this region (Fig. 3a, d and e, green boxes). Iron also emerges as a potential driver of PP decreases within the 50–65° S band, but not across all of the models (Fig. 3c, green box). An increase in both IPAR and iron supply across the models results in PP increases south of 65° S, as highlighted by the orange boxes in Fig. 3c and Fig. 3d. Models IPSL-CM5A-LR, IPSL-CM5A-MR, and GFDL-ESM2G deviate from this trend slightly in that they experience small relative decreases in IPAR south of 65° S, while still experiencing increases in PP. However, these three models also exhibit shoaling of the summertime MLD here, which would increase light availability, likely canceling the effects of decreased IPAR at the surface. Note that for all models except for the three just mentioned, IPAR increases despite an increase in cloud cover (Fig. 3e, orange dots). This suggests that sea ice fraction, rather than cloud cover, is the most important factor in determining IPAR in this region. As sea ice cover declines near the Antarctic continent within the models, more light is able to reach the ocean surface, ultimately leading to increased IPAR and PP here.

While general agreement on the mechanisms driving 100-year phytoplankton changes among models is high, one noteworthy result is that there appear to be two distinct groups of models: one group with phytoplankton which are highly sensitive to changes in iron concentrations south of ~ 40° S (consisting of GFDL-ESM2, CESM1-BGC, IPSL-CM5A, CMCC-CESM – see Fig. S11, for models where zonal PB or PP changes closely follow zonal iron changes) and a second group with phytoplankton which are less iron-sensitive (NorESM1-ME, HadGEM2, GISS-E2, MPI-ESM) or do not include iron at all (CanESM2, MIROC-ESM, MRI-ESM1). Models within the first group tend to exhibit less well-defined latitudinally-banded 100-year phytoplankton changes, while models within the second group tend to exhibit a more obviously banded PB and PP change structure (see Figs. S1–2). Models within this latter group also frequently display iron and phytoplankton changes of opposite signs south of 40° S (Fig. 4c, un-

BGD

12, 8157–8197, 2015

A latitudinally-banded phytoplankton response

S. Leung et al.

Title Page

Abstract

Introduction

Conclusions

References

Tables

Figures

◀

▶

◀

▶

Back

Close

Full Screen / Esc

Printer-friendly Version

Interactive Discussion



A latitudinally-banded phytoplankton response

S. Leung et al.

Title Page

Abstract

Introduction

Conclusions

References

Tables

Figures



Back

Close

Full Screen / Esc

Printer-friendly Version

Interactive Discussion



will weaken here, shoaling the MLD and prolonging the growing season by allowing phytoplankton to remain within the well-lit surface layers for longer. Thus, enhanced future phytoplankton populations within this transitional band are not unexpected. Within the subpolar (50° S to 65° S) band, models are not as consistent in their predictions of phytoplankton changes compared with the other regions. Only 41 % of model realizations predict a decrease in PP, while 55 % predict a decrease in PB. Predicted changes in driving variables are somewhat more consistent within this region, however, with a decrease in summertime MLD predicted by 56 % of model realizations, an increase in cloud cover predicted by 60 %, and a decrease in IPAR predicted by 71 %. With a projected poleward shift of the westerlies, cloud cover should increase (due to a concomitant shift in storm-track cloudiness and/or altered tropospheric stability with future warming) and MLDs should deepen as winds intensify within this band, both of which act to decrease phytoplankton populations, exactly as we see here. Within the Antarctic (south of 65° S) band, 76 % of model realizations predict an increase in PP, while 64 % predict an increase in PB, both of which are associated with projected increases in wintertime iron concentrations (72 %) and summertime light availability (59 %). This goes with our expectation that the melting of sea ice projected by the models will lead to higher amounts of light reaching the ocean surface and that intensified westerlies will bring a larger supply of upwelled iron to the surface in this region, both of which act to increase phytoplankton populations, just as we see here.

To get a wider sense of spatial agreement among models, Fig. S16 shows the consistency of modeled trends in all variables at each grid point within the SO using the same bootstrap technique as in Fig. 5 (i.e., Fig. 5 is just Fig. S16 spatially averaged over each zonal band). From Fig. S16, one can see that agreement among models is highest at the center of each zonal band, but decreases toward the edges due to offsets in the precise boundaries of water masses among the models. These slight offsets lower the zonal band-average agreement among models as presented in Fig. 5, such that if one were able to perfectly compare water masses among models, consis-

tency in predicted trends (as measured by percentage of model realizations projecting a change in the same direction) would likely be even higher.

3.4 Linking CMIP5 model projections to observations

We now ask how our modeled projections compare to observed trends thus far. The SO satellite chl record is not yet long enough to separate the effects of climate change from those of interannual processes driven by the leading modes of shorter-term variability in the SO (e.g., Boyd et al., 2008; Strutton et al., 2012; Henson et al., 2010; Beaulieu et al., 2013), the most important being the SAM (Thompson and Solomon, 2002). In-situ data from field campaigns suffer from the same temporal constraint. For this reason, many observational studies have looked at the effects of these modes of variability, rather than climate change, on phytoplankton abundance and productivity. These types of studies can, however, still provide essential insight into the mechanisms driving possible longer-term changes. For example, as was mentioned before, the SAM index is expected to become increasingly positive as SO westerlies strengthen and move poleward with future warming (see Fig. S10 for projected SAM time series within the CMIP5 models). We have shown here that at least within the CMIP5 models, mechanisms responsible for changes in phytoplankton biomass on interannual and 5-year time scales are also responsible for projected 100-year trends within the SO. Thus, understanding the effects of a more positive SAM on SO phytoplankton may help predict the direction of phytoplankton changes in a warmer future climate. An important caveat to keep in mind when looking at observational data, however, is that observations rarely span consistent timeframes, making it difficult to compare studies in a perfectly congruent way. For instance, it has been shown that the magnitude and sign of observed trends can be very sensitive to the start and end years analyzed (Fay et al., 2014). Thus, rather than directly comparing recently observed trends with 21st century CMIP5 projections, we seek only to qualitatively understand whether there are common mechanisms and directions of change within the observational data and model projections. The studies

BGD

12, 8157–8197, 2015

A latitudinally-banded phytoplankton response

S. Leung et al.

Title Page

Abstract

Introduction

Conclusions

References

Tables

Figures

◀

▶

◀

▶

Back

Close

Full Screen / Esc

Printer-friendly Version

Interactive Discussion



cited in the following paragraphs are visually and tabularly summarized in Fig. 6 and Table S3.

Analyzing satellite data over years 1997–2004, Lovenduski and Gruber (2005) (LG2005) found a negative correlation (though not significant) between SAM and chl concentrations within the SO Subtropical Zone ($\sim 30\text{--}40^\circ\text{S}$), due to increased stratification and decreased upwelling of macronutrients during positive SAM periods. Assuming that SAM will continue to increase with future warming and that the same driving mechanisms will hold on timescales ranging from interannual to centennial, phytoplankton biomass would be expected to decrease over the 21st century within the Subtropical Zone ($\sim 30\text{--}40^\circ\text{S}$) due to enhanced macronutrient limitation, which is indeed what the CMIP5 models predict.

Via a combination of satellite, reanalysis, and model data, Johnston and Gabric (2011) (JG2011) found that both summertime chl concentrations and primary productivity increased within the Australian sector between $40\text{--}50^\circ\text{S}$ over the years 1997–2007, which they attribute to increased water column stratification or enhanced mineral dust deposition from Australia. Gregg et al. (2005) (G2005) likewise found an increase in chl concentrations just south of Australia ($\sim 35\text{--}55^\circ\text{S}$) from satellite data over the period 1998–2003, accompanied by an increase in springtime SST, likely associated with a shoaling of the mixed layer. Using satellite chl concentrations (1997–2010) calculated in two different ways, Siegel et al. (2013) (S2013) also reported an increase in chl concentrations between $\sim 40\text{--}50^\circ\text{S}$. These proposed mechanisms and directions of trends are consistent with those of the CMIP5 models, which predict that increased dissolved iron concentrations together with decreased light limitation due to shallower MLDs during blooms will drive 21st century phytoplankton increases within the $40\text{--}50^\circ\text{S}$ band.

From satellite data (1997–2004), LG2005 found a significant negative correlation between SAM and chl concentrations within the \sim mid-40 to mid- 50°S latitudes below Australia, which they ascribe to increased light limitation due to deeper summertime mixed layers in positive SAM phases. Consistent with LG2005 and an increasingly

BGD

12, 8157–8197, 2015

A
latitudinally-banded
phytoplankton
response

S. Leung et al.

Title Page

Abstract

Introduction

Conclusions

References

Tables

Figures

◀

▶

◀

▶

Back

Close

Full Screen / Esc

Printer-friendly Version

Interactive Discussion



A latitudinally-banded phytoplankton response

S. Leung et al.

[Title Page](#)[Abstract](#)[Introduction](#)[Conclusions](#)[References](#)[Tables](#)[Figures](#)[Back](#)[Close](#)[Full Screen / Esc](#)[Printer-friendly Version](#)[Interactive Discussion](#)

in cloudiness and wind intensity and an increase in the number of ice-free summer days. Meanwhile, S2013 observed a thin band of chl increase around $\sim 65^\circ$ S over the years 1997–2010. These observations are also consistent with future CMIP5 model projections, which predict that decreased sea ice cover will drive phytoplankton abundance increases south of $\sim 65^\circ$ S in spite of an increase in cloud cover (contrary to the decrease in cloudiness measured by MH2009). Lastly, Smith and Comiso (2008) (SC2008) calculate an increase in annual primary productivity over the entire Southern Ocean (defined as south of 60° S) between 1997 and 2006, while Arrigo et al. (2008) (A2008) calculate no significant trend over the same period. The discrepancy between these two works is partly due to the fact that A2008 define the Southern Ocean as south of 50° S instead of 60° S, and the region in between 50 – 60° S underwent a decrease in productivity over both studies' time periods (reducing the magnitude of the increasing trend over the rest of the SO), again consistent with model projections of future phytoplankton biomass decrease between 50 – 65° S and increase south of 65° S.

In general, observed spatial distributions in SO chl trends over the SeaWiFS (Sea-viewing Wide Field-of-view Sensor) period (1997–2010) (Fig. 6b and c) correspond well with CMIP5 all-model mean projections (Fig. 1a and b), with the largest observed chl increases occurring between ~ 40 – 50° S and south of $\sim 65^\circ$ S and decreases occurring between ~ 50 – 65° S. Latitudinally-banded trends in reanalysis products of summertime MLD and cloud cover over recent decades also correspond well with CMIP5 model projections. For example, the largest observed increases in summertime MLD (over the years 1950–2013) and cloud cover (over the years 1980–2013) occur south of $\sim 50^\circ$ S, while the largest decreases occur north of $\sim 50^\circ$ S (Fig. 6d and e compared with Fig. 1d and g, respectively).

In summary, the observed spatial distribution in trends of phytoplankton productivity, MLD, and cloud cover over the past few decades qualitatively matches the latitudinally-banded structure of the respective 100-year future trends predicted by the CMIP5 models. This potentially suggests that the effects of climate change on SO phytoplankton may have already become detectable. Furthermore, the fact that these long-term model

projections also appear to agree with the sign of observed SAM-driven effects throughout the SO suggests that an increasingly positive SAM may be responsible for the predicted zonally-banded pattern of phytoplankton biomass changes in the models, though further work is needed to precisely quantify SAM's contribution to PB and PP changes within the CMIP5 model suite (Leung et al., 2015).

4 Conclusions

The 16 CMIP5 models with explicit phytoplankton ecology predict a zonally-banded pattern of 21st century phytoplankton biomass and productivity changes within the Southern Ocean: a decrease in the subtropical band ($\sim 30\text{--}40^\circ\text{S}$), an increase in the transitional band ($\sim 40\text{--}50^\circ\text{S}$), a decrease in the subpolar band ($\sim 50\text{--}65^\circ\text{S}$), and an increase in the Antarctic band (south of $\sim 65^\circ\text{S}$). In line with theoretical expectations and previous modeling studies, light (controlled by cloud cover, summertime MLD during blooms, and sea ice fraction) and iron supply are found to be the most important driving factors of phytoplankton changes in the transitional and subpolar Southern Ocean (south of $\sim 40^\circ\text{S}$), while nitrate is found to be the most important driving factor in the subtropical Southern Ocean ($\sim 30\text{--}40^\circ\text{S}$). Shifts in these driving variables consistently bring about changes in phytoplankton abundance and production on multiple relevant timescales. In particular, within a given zonally-banded biome in an individual model, the same mechanisms are generally responsible for phytoplankton biomass changes on an interannual, decadal, and 100-year basis. This suggests that the mechanisms driving shorter-term phytoplankton variability and which can in principle be gaged from in-situ or satellite observations are also likely to be the mechanisms responsible for climate-driven phytoplankton changes over the 21st century. Furthermore, 21st century trends in phytoplankton productivity predicted by the CMIP5 models go in the same direction as observed trends over the last couple of decades and tentatively agree with the sign of established SAM-driven changes. This suggests that an increasingly positive SAM may be responsible for the projected zonally-banded trends in phytoplankton

productivity and biomass that we observe in the CMIP5 models, though more work is needed to carefully test this hypothesis.

With such short observational records, our model-observational data intercomparison is clearly only qualitative at this point in time. We advocate for longer in-situ phytoplankton biomass and satellite chl data collection in this important but massively under-sampled region of the world ocean to allow for the emergence of a climate change signal from interannual variability. The main result of this study – a consistency of the model-projected phytoplankton trends within 4 distinct SO bands over the 21st century – suggests a mechanism for selecting a minimal number of sites for future SO biogeochemical observational time series stations; at a minimum, one or two representative time series are needed from each of the 4 SO bands described.

Follow-up work is needed to determine how the projected changes in phytoplankton biomass and productivity will affect SO carbon and nutrient cycling, as well as how changes in the characteristics of regional SO seasonality can affect these long-term trends (Thomalla et al., 2011). Driving higher trophic level models with projected CMIP5 phytoplankton abundances may also yield important insights into how ecologically and economically important species such as zooplankton, krill, marine mammals, penguins, and seabirds will respond to climate change. Given the fragility of polar ecosystems and the critical importance of the SO in driving global carbon and nutrient cycles as well as low-latitude productivity, our results highlight the need for both long-term in-situ and satellite monitoring of Southern Ocean biology and biogeochemistry.

**The Supplement related to this article is available online at
doi:10.5194/bgd-12-8157-2015-supplement.**

Acknowledgements. A. Cabré and I. Marinov acknowledge support by NASA ROSES grant NNX13AC92G and a University of Pennsylvania research foundation grant.

BGD

12, 8157–8197, 2015

A
latitudinally-banded
phytoplankton
response

S. Leung et al.

Title Page

Abstract

Introduction

Conclusions

References

Tables

Figures

◀

▶

◀

▶

Back

Close

Full Screen / Esc

Printer-friendly Version

Interactive Discussion



References

- Arblaster, J. M. and Meehl, G. A.: Contributions of external forcings to southern annular mode trends, *J. Climate*, 19, 2896–2905, doi:10.1175/jcli3774.1, 2006.
- Arrigo, K. R., van Dijken, G. L., and Bushinsky, S.: Primary production in the Southern Ocean, 1997–2006, *J. Geophys. Res.-Oceans*, 113, C08004, doi:10.1029/2007jc004551, 2008.
- Assmann, K. M., Bentsen, M., Segschneider, J., and Heinze, C.: An isopycnic ocean carbon cycle model, *Geosci. Model Dev.*, 3, 143–167, doi:10.5194/gmd-3-143-2010, 2010.
- Atkinson, A., Siegel, V., Pakhomov, E., and Rothery, P.: Long-term decline in krill stock and increase in salps within the Southern Ocean, *Nature*, 432, 100–103, doi:10.1038/nature02950, 2004.
- Aumont, O. and Bopp, L.: Globalizing results from ocean in situ iron fertilization studies, *Global Biogeochem. Cy.*, 20, doi:10.1029/2005gb002591, 2006.
- Ayers, J. M. and Strutton, P. G.: Nutrient availability in Subantarctic Mode Waters forced by the Southern Annular Mode and ENSO, *Geophys. Res. Lett.*, 40, 3419–3423, 2013.
- Beaulieu, C., Henson, S. A., Sarmiento, Jorge L., Dunne, J. P., Doney, S. C., Rykaczewski, R. R., and Bopp, L.: Factors challenging our ability to detect long-term trends in ocean chlorophyll, *Biogeosciences*, 10, 2711–2724, doi:10.5194/bg-10-2711-2013, 2013.
- Bender, F. A. M., Ramanathan, V., and Tselioudis, G.: Changes in extratropical storm track cloudiness 1983–2008: observational support for a poleward shift, *Clim. Dynam.*, 38, 2037–2053, doi:10.1007/s00382-011-1065-6, 2012.
- Bopp, L., Monfray, P., Aumont, O., Dufresne, J. L., Le Treut, H., Madec, G., Terray, L., and Orr, J. C.: Potential impact of climate change on marine export production, *Global Biogeochem. Cy.*, 15, 81–99, doi:10.1029/1999gb001256, 2001.
- Bopp, L., Aumont, O., Cadule, P., Alvain, S., and Gehlen, M.: Response of diatoms distribution to global warming and potential implications: a global model study, *Geophys. Res. Lett.*, 32, L19606, doi:10.1029/2005gl023653, 2005.
- Bopp, L., Resplandy, L., Orr, J. C., Doney, S. C., Dunne, J. P., Gehlen, M., Halloran, P., Heinze, C., Ilyina, T., Séférian, R., Tjiputra, J., and Vichi, M.: Multiple stressors of ocean ecosystems in the 21st century: projections with CMIP5 models, *Biogeosciences*, 10, 6225–6245, doi:10.5194/bg-10-6225-2013, 2013.
- Boyd, P. W., Crossley, A. C., DiTullio, G. R., Griffiths, F. B., Hutchins, D. A., Queguiner, B., Sedwick, P. N., and Trull, T. W.: Control of phytoplankton growth by iron supply and irradiance

BGD

12, 8157–8197, 2015

A latitudinally-banded phytoplankton response

S. Leung et al.

Title Page

Abstract

Introduction

Conclusions

References

Tables

Figures

◀

▶

◀

▶

Back

Close

Full Screen / Esc

Printer-friendly Version

Interactive Discussion



A latitudinally-banded phytoplankton response

S. Leung et al.

[Title Page](#)
[Abstract](#)
[Introduction](#)
[Conclusions](#)
[References](#)
[Tables](#)
[Figures](#)




[Back](#)
[Close](#)
[Full Screen / Esc](#)
[Printer-friendly Version](#)
[Interactive Discussion](#)


in the subantarctic Southern Ocean: experimental results from the SAZ Project, *J. Geophys. Res.-Oceans*, 106, 31573–31583, doi:10.1029/2000jc000348, 2001.

Boyd, P. W., Doney, S. C., Strzepek, R., Dusenberry, J., Lindsay, K., and Fung, I.: Climate-mediated changes to mixed-layer properties in the Southern Ocean: assessing the phytoplankton response, *Biogeosciences*, 5, 847–864, doi:10.5194/bg-5-847-2008, 2008.

Cabré, A., Marinov, I., and Leung, S.: Consistent global responses of marine ecosystems to future climate change across the IPCC AR5 earth system models, *Clim. Dynam.*, 1–28, doi:10.1007/s00382-014-2374-3, 2014.

Ceppi, P., Zelinka, M. D., and Hartmann, D. L.: The response of the Southern Hemispheric eddy-driven jet to future changes in shortwave radiation in CMIP5, *Geophys. Res. Lett.*, 41, 3244–3250, doi:10.1002/2014gl060043, 2014.

Cullen, J. J.: Hypotheses to explain high-nutrient conditions in the open sea, *Limnol. Oceanogr.*, 36, 1578–1599, 1991.

Doney, S. C.: Oceanography – plankton in a warmer world, *Nature*, 444, 695–696, doi:10.1038/444695a, 2006.

Dunne, J. P., John, J. G., Shevliakova, E., Stouffer, R. J., Krasting, J. P., Malyshev, S. L., Milly, P. C. D., Sentman, L. T., Adcroft, A. J., Cooke, W., Dunne, K. A., Griffies, S. M., Hallberg, R. W., Harrison, M. J., Levy, H., Wittenberg, A. T., Phillips, P. J., and Zadeh, N.: GFDL's ESM2 Global Coupled Climate-Carbon Earth System Models. Part II: carbon system formulation and baseline simulation characteristics, *J. Climate*, 26, 2247–2267, doi:10.1175/jcli-d-12-00150.1, 2013.

Eppley, R. W. and Peterson, B. J.: Particulate organic-matter flux and planktonic new production in the deep ocean, *Nature*, 282, 677–680, doi:10.1038/282677a0, 1979.

Falkowski, P., Scholes, R. J., Boyle, E., Canadell, J., Canfield, D., Elser, J., Gruber, N., Hibbard, K., Hogberg, P., Linder, S., Mackenzie, F. T., Moore, B., Pedersen, T., Rosenthal, Y., Seitzinger, S., Smetacek, V., and Steffen, W.: The global carbon cycle: a test of our knowledge of earth as a system, *Science*, 290, 291–296, doi:10.1126/science.290.5490.291, 2000.

Fay, A. R., McKinley, G. A., and Lovenduski, N. S.: Southern Ocean carbon trends: sensitivity to methods, *Geophys. Res. Lett.*, 41, 6833–6840, doi:10.1002/2014gl061324, 2014.

Feng, Y., Hare, C. E., Rose, J. M., Handy, S. M., DiTullio, G. R., Lee, P. A., Smith, W. O., Jr., Peloquin, J., Tozzi, S., Sun, J., Zhang, Y., Dunbar, R. B., Long, M. C., Sohst, B., Lohan, M.,

A latitudinally-banded phytoplankton response

S. Leung et al.

[Title Page](#)
[Abstract](#)
[Introduction](#)
[Conclusions](#)
[References](#)
[Tables](#)
[Figures](#)
[Back](#)
[Close](#)
[Full Screen / Esc](#)
[Printer-friendly Version](#)
[Interactive Discussion](#)


- and Hutchins, D. A.: Interactive effects of iron, irradiance and CO₂ on Ross Sea phytoplankton, *Deep-Sea Res. Pt. I*, 57, 368–383, doi:10.1016/j.dsr.2009.10.013, 2010. (FOUND!)
- Geider, R. J., Delucia, E. H., Falkowski, P. G., Finzi, A. C., Grime, J. P., Grace, J., Kana, T. M., La Roche, J., Long, S. P., Osborne, B. A., Platt, T., Prentice, I. C., Raven, J. A., Schlesinger, W. H., Smetacek, V., Stuart, V., Sathyendranath, S., Thomas, R. B., Vogelmann, T. C., Williams, P., and Woodward, F. I.: Primary productivity of planet earth: biological determinants and physical constraints in terrestrial and aquatic habitats, *Glob. Change Biol.*, 7, 849–882, doi:10.1046/j.1365-2486.2001.00448.x, 2001.
- Gillett, N. P. and Fyfe, J. C.: Annular mode changes in the CMIP5 simulations, *Geophys. Res. Lett.*, 40, 1189–1193, doi:10.1002/grl.50249, 2013.
- Gregg, W. W.: Assimilation of SeaWiFS ocean chlorophyll data into a three-dimensional global ocean model, *J. Marine Syst.*, 69, 205–225, doi:10.1016/j.jmarsys.2006.02.015, 2008.
- Gregg, W. W., Casey, N. W., and McClain, C. R.: Recent trends in global ocean chlorophyll, *Geophys. Res. Lett.*, 32, L03606, doi:10.1029/2004gl021808, 2005.
- Heinze, C., Maier-Reimer, E., and Winn, K.: Glacial pCO₂ reduction by the World Ocean: experiments with the Hamburg Carbon Cycle Model, *Paleoceanography*, 6, 395–430, 1991.
- Henson, S. A., Sarmiento, J. L., Dunne, J. P., Bopp, L., Lima, I., Doney, S. C., John, J., and Beaulieu, C.: Detection of anthropogenic climate change in satellite records of ocean chlorophyll and productivity, *Biogeosciences*, 7, 621–640, doi:10.5194/bg-7-621-2010, 2010.
- Ilyina, T., Six, K. D., Segschneider, J., Maier-Reimer, E., Li, H., and Nunez-Riboni, I.: Global ocean biogeochemistry model HAMOCC: model architecture and performance as component of the MPI-Earth system model in different CMIP5 experimental realizations, *J. Adv. Model. Earth Syst.*, 5, 287–315, doi:10.1029/2012ms000178, 2013.
- Johnston, B. M. and Gabric, A. J.: Interannual variability in estimated biological productivity in the Australian sector of the Southern Ocean in 1997–2007, *Tellus B*, 63, 266–286, doi:10.1111/j.1600-0889.2011.00526.x, 2011.
- Kay, J. E., Medeiros, B., Hwang, Y. T., Gettelman, A., Perket, J., and Flanner, M. G.: Processes controlling Southern Ocean shortwave climate feedbacks in CESM, *Geophys. Res. Lett.*, 41, 616–622, doi:10.1002/2013gl058315, 2014.
- Laufkötter, C., Vogt, M., Gruber, N., Aita-Noguchi, M., Aumont, O., Bopp, L., Buitenhuis, E., Doney, S. C., Dunne, J., Hashioka, T., Hauck, J., Hirata, T., John, J., Le Quéré, C., Lima, I. D., Nakano, H., Seferian, R., Totterdell, I., Vichi, M., and Völker, C.: Drivers and uncertainties

A latitudinally-banded phytoplankton response

S. Leung et al.

[Title Page](#)
[Abstract](#)
[Introduction](#)
[Conclusions](#)
[References](#)
[Tables](#)
[Figures](#)




[Back](#)
[Close](#)
[Full Screen / Esc](#)
[Printer-friendly Version](#)
[Interactive Discussion](#)


of future global marine primary production in marine ecosystem models, *Biogeosciences Discuss.*, 12, 3731–3824, doi:10.5194/bgd-12-3731-2015, 2015.

Le Quéré, C., Harrison, S. P., Prentice, I. C., Buitenhuis, E. T., Aumont, O., Bopp, L., Claustre, H., Da Cunha, L. C., Geider, R., Giraud, X., Klaas, C., Kohfeld, K. E., Legendre, L., Manizza, M., Platt, T., Rivkin, R. B., Sathyendranath, S., Uitz, J., Watson, A. J., and Wolf-Gladrow, D.: Ecosystem dynamics based on plankton functional types for global ocean biogeochemistry models, *Glob. Change Biol.*, 11, 2016–2040, doi:10.1111/j.1365-2468.2005.01004.x, 2005.

Leung, S., Cabré, A., and Marinov, I.: The effects of the Southern Annular Mode on phytoplankton production within the CMIP5 model suite and implications for future climate change, in preparation, 2015.

Lovenduski, N. S. and Gruber, N.: Impact of the Southern Annular Mode on Southern Ocean circulation and biology, *Geophys. Res. Lett.*, 32, L11603, doi:10.1029/2005gl022727, 2005.

Marinov, I., Gnanadesikan, A., Toggweiler, J. R., and Sarmiento, J. L.: The Southern Ocean biogeochemical divide, *Nature*, 441, 964–967, doi:10.1038/nature04883, 2006.

Marinov, I., Doney, S. C., and Lima, I. D.: Response of ocean phytoplankton community structure to climate change over the 21st century: partitioning the effects of nutrients, temperature and light, *Biogeosciences*, 7, 3941–3959, doi:10.5194/bg-7-3941-2010, 2010.

Marinov, I., Doney, S. C., Lima, I. D., Lindsay, K., Moore, J. K., and Mahowald, N.: North–South asymmetry in the modeled phytoplankton community response to climate change over the 21st century, *Global Biogeochem. Cy.*, 27, 1274–1290, doi:10.1002/2013gb004599, 2013.

Martin, J. H., Gordon, R. M., and Fitzwater, S. E.: Iron in Antarctic waters, *Nature*, 345, 156–158, doi:10.1038/345156a0, 1990.

Meijers, A. J. S., Shuckburgh, E., Bruneau, N., Sallee, J. B., Bracegirdle, T. J., and Wang, Z.: Representation of the Antarctic Circumpolar Current in the CMIP5 climate models and future changes under warming scenarios, *J. Geophys. Res.-Oceans*, 117, C12008, doi:10.1029/2012jc008412, 2012.

Montes-Hugo, M., Doney, S. C., Ducklow, H. W., Fraser, W., Martinson, D., Stammerjohn, S. E., and Schofield, O.: Recent changes in phytoplankton communities associated with rapid regional climate change along the Western Antarctic Peninsula, *Science*, 323, 1470–1473, doi:10.1126/science.1164533, 2009.

Moore, C. M., Mills, M. M., Arrigo, K. R., Berman-Frank, I., Bopp, L., Boyd, P. W., Galbraith, E. D., Geider, R. J., Guieu, C., Jaccard, S. L., Jickells, T. D., La Roche, J., Lenton, T. M.,

A latitudinally-banded phytoplankton response

S. Leung et al.

[Title Page](#)
[Abstract](#)
[Introduction](#)
[Conclusions](#)
[References](#)
[Tables](#)
[Figures](#)
[Back](#)
[Close](#)
[Full Screen / Esc](#)
[Printer-friendly Version](#)
[Interactive Discussion](#)


- Mahowald, N. M., Maranon, E., Marinov, I., Moore, J. K., Nakatsuka, T., Oschlies, A., Saito, M. A., Thingstad, T. F., Tsuda, A., and Ulloa, O.: Processes and patterns of oceanic nutrient limitation, *Nat. Geosci.*, 6, 701–710, doi:10.1038/ngeo1765, 2013.
- Moore, J. K., Doney, S. C., and Lindsay, K.: Upper ocean ecosystem dynamics and iron cycling in a global three-dimensional model, *Global Biogeochem. Cy.*, 18, GB4028, doi:10.1029/2004gb002220, 2004.
- Moore, J. K., Doney, S. C., Lindsay, K., Mahowald, N., and Michaels, A. F.: Nitrogen fixation amplifies the ocean biogeochemical response to decadal timescale variations in mineral dust deposition, *Tellus B*, 58, 560–572, doi:10.1111/j.1600-0889.2006.00209.x, 2006.
- Palmer, J. R. and Totterdell, I. J.: Production and export in a global ocean ecosystem model, *Deep-Sea Res. Pt. I*, 48, 1169–1198, doi:10.1016/s0967-0637(00)00080-7, 2001. (FOUND!)
- Pitchford, J. W. and Brindley, J.: Iron limitation, grazing pressure and oceanic high nutrient-low chlorophyll (HNLC) regions, *J. Plankton Res.*, 21, 525–547, doi:10.1093/plankt/21.3.525, 1999.
- Russell, J. L., Dixon, K. W., Gnanadesikan, A., Stouffer, R. J., and Toggweiler, J. R.: The Southern Hemisphere westerlies in a warming world: propping open the door to the deep ocean, *J. Climate*, 19, 6382–6390, doi:10.1175/jcli3984.1, 2006.
- Sarmiento, J. L., Gruber, N., Brzezinski, M. A., and Dunne, J. P.: High-latitude controls of thermocline nutrients and low latitude biological productivity, *Nature*, 427, 56–60, doi:10.1038/nature02127, 2004a.
- Sarmiento, J. L., Slater, R., Barber, R., Bopp, L., Doney, S. C., Hirst, A. C., Kleypas, J., Matear, R., Mikolajewicz, U., Monfray, P., Soldatov, V., Spall, S. A., and Stouffer, R.: Response of ocean ecosystems to climate warming, *Global Biogeochem. Cy.*, 18, GB3003, doi:10.1029/2003gb002134, 2004b.
- Schmittner, A., Oschlies, A., Matthews, H. D., and Galbraith, E. D.: Future changes in climate, ocean circulation, ecosystems, and biogeochemical cycling simulated for a business-as-usual CO₂ emission scenario until year 4000 AD, *Global Biogeochem. Cy.*, 22, GB1013, doi:10.1029/2007gb002953, 2008.
- Seferian, R., Bopp, L., Gehlen, M., Orr, J. C., Ethe, C., Cadule, P., Aumont, O., Salas y Melia, D., Voldoire, A., and Madec, G.: Skill assessment of three earth system models with common marine biogeochemistry, *Clim. Dynam.*, 40, 2549–2573, doi:10.1007/s00382-012-1362-8, 2013.

A latitudinally-banded phytoplankton response

S. Leung et al.

[Title Page](#)
[Abstract](#)
[Introduction](#)
[Conclusions](#)
[References](#)
[Tables](#)
[Figures](#)
[Back](#)
[Close](#)
[Full Screen / Esc](#)
[Printer-friendly Version](#)
[Interactive Discussion](#)


and Rose, S. K.: The representative concentration pathways: an overview, *Climatic Change*, 109, 5–31, doi:10.1007/s10584-011-0148-z, 2011.

Vichi, M., Pinardi, N., and Masina, S.: A generalized model of pelagic biogeochemistry for the global ocean ecosystem. Part I: Theory, *J. Marine Syst.*, 64, 89–109, doi:10.1016/j.jmarsys.2006.03.006, 2007.

Wang, S. and Moore, J. K.: Variability of primary production and air–sea CO₂ flux in the Southern Ocean, *Global Biogeochem. Cy.*, 26, GB1008, doi:10.1029/2010gb003981, 2012.

Watanabe, S., Hajima, T., Sudo, K., Nagashima, T., Takemura, T., Okajima, H., Nozawa, T., Kawase, H., Abe, M., Yokohata, T., Ise, T., Sato, H., Kato, E., Takata, K., Emori, S., and Kawamiya, M.: MIROC-ESM 2010: model description and basic results of CMIP5-20c3m experiments, *Geosci. Model Dev.*, 4, 845–872, doi:10.5194/gmd-4-845-2011, 2011.

Yin, J. H.: A consistent poleward shift of the storm tracks in simulations of 21st century climate, *Geophys. Res. Lett.*, 32, L18701, doi:10.1029/2005gl023684, 2005.

Yukimoto, S., Yoshimura, H., Hosaka, M., Sakami, T., Tsujino, H., Hirabara, M., Tanaka, T. Y., Deushi, M., Obata, A., Nakano, H., Adachi, Y., Shindo, E., Yabu, S., Ose, T., and Kitoh, A.: MRI-ESM1 model description, Technical reports of the Meteorological Research Institute, 64, available at: http://www.mri-jma.go.jp/Publish/Technical/DATA/VOL_64/tec_rep_mri_64.pdf, 2011.

Zahariev, K., Christian, J. R., and Denman, K. L.: Preindustrial, historical, and fertilization simulations using a global ocean carbon model with new parameterizations of iron limitation, calcification, and N-2 fixation, *Prog. Oceanogr.*, 77, 56–82, doi:10.1016/j.pocean.2008.01.007, 2008.

Zheng, F., Li, J., Clark, R. T., and Nnamchi, H. C.: Simulation and Projection of the Southern Hemisphere Annular Mode in CMIP5 Models, *J. Climate*, 26, 9860–9879, doi:10.1175/jcli-d-13-00204.1, 2013.

Table 1. CMIP5 model details. Summary of all the CMIP5 models that keep track of phytoplankton biomass and primary production with information on the following for each model: spatial resolution in the atmosphere and ocean, explicitly modeled nutrients, ecology subroutine, references, and weight applied in the all-model averages.

Model	Atm (levels, lon/lat)	Ocean (levels, lon/lat)	Nutrients	Ecology module	Reference	Wt.
CanESM2	L35 2.8/2.8	L40 1.4/0.9	N (but also accounts for Fe limitation)	NPZD Denman and Peña (1999)	Zahariev et al. (2008) ⁴⁰	1
CESM1-BGC	L26 1.25/0.94	L60 1.125/0.27–0.53	(P), N, Fe, Si	MET	Moore et al. (2004) ⁴¹ ; Moore et al. (2006) ⁴²	1
CMCC-CESM	L39 3.8/3.7	L31 2/0.5–2	(P), N, Fe, Si	PELAGOS	Vichi et al. (2007) ⁴³	0*
GFDL-ESM2G	L24 2.5/2.0	L63 1/0.3–1	P, N, Fe, Si	TOPAZ2	Dunne et al. (2013) ⁴⁴	1
GFDL-ESM2M	L24 2.5/2.0	L50 1/0.3–1	P, N, Fe, Si	TOPAZ2	Dunne et al. (2013) ⁴⁴	1
HadGEM2-CC	L60 1.25/1.875	L40 1/0.3–1	N, Fe, Si	Diat- HadOCC (NPZD)	Palmer and Totterdell (2001) ⁴⁵	0.5
HadGEM2-ES	L38 1.25/1.875	L40 1/0.3–1	N, Fe, Si	Diat- HadOCC (NPZD)	Palmer and Totterdell (2001) ⁴⁵	0.5
IPSL-CM5A-LR	L39 3.75/1.875	L31 2/0.5–2	P, N, Fe, Si	PISCES (from HAMOCC5)	Aumont and Bopp (2006) ⁴⁶ ; Séférian et al. (2013) ⁴⁷	0.5
IPSL-CM5A-MR	L39 2.5/1.25	L31 2/0.5–2	P, N, Fe, Si	PISCES (from HAMOCC5)	Aumont and Bopp (2006) ⁴⁶ ; Séférian et al. (2013) ⁴⁷	0.5
MIROC-ESM	L80 2.8	L44 1.4/0.5–1.7	N	NPZD-type Oschlies (2001)	Watanabe et al. (2006) ⁴⁸	0.5
MIROC-ESM-CHEM	L80 2.8	L44 1.4/0.5–1.7	N	NPZD-type Oschlies (2001)	Watanabe et al. (2006) ⁴⁸	0.5
MPI-ESM-MR	L47 1.9	L40 0.4	P, N, Fe, Si	HAMOCC5.2 (NPZD)	Ilyina et al. (2013) ⁴⁹	0.5
MPI-ESM-LR	L47 1.9	L40 1.5	P, N, Fe, Si	HAMOCC5.2 (NPZD)	Ilyina et al. (2013) ⁴⁹	0.5
MRI-ESM1	L23 1.125/1.121	L51 1/0.5	P, N	NPZD Oschlies (2001)	Yukimoto et al. (2011) ⁵⁰	1
NorESM1-ME	L26 1.9/2.5	L53 1/1.25	P, N, Fe, Si	HAMOCC5.1 (NPZD)	Assmann et al. (2010) ⁵¹	1
GISS-E2-H-CC	L40 2.5/2	L26 1/1	N, Fe, Si	NOBM	Gregg (2008) ⁵²	1
GISS-E2-R-CC	L40 2.5/2	L32 1.25/1	N, Fe, Si	NOBM	Gregg (2008) ⁵²	1

* Note: CMCC-CESM runs did not appear to reach equilibrium, which was a necessary condition we imposed in order to work with a model; thus, we only show CMCC-CESM data in the supplementary figures, but do not take it into account in the all-model averages.

A
latitudinally-banded
phytoplankton
response

S. Leung et al.

Title Page

Abstract

Introduction

Conclusions

References

Tables

Figures



Back

Close

Full Screen / Esc

Printer-friendly Version

Interactive Discussion



A latitudinally-banded phytoplankton response

S. Leung et al.

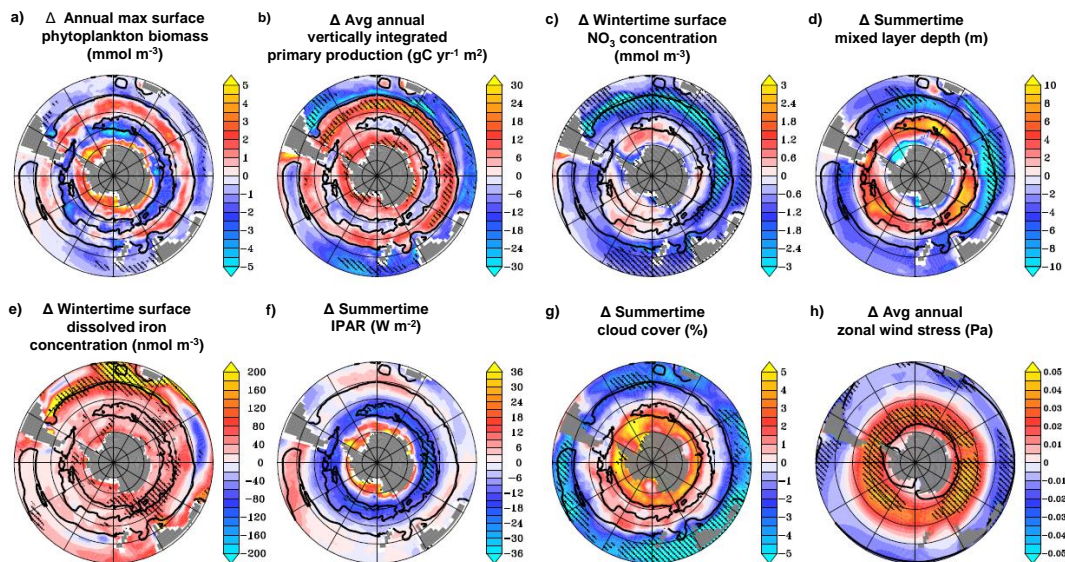
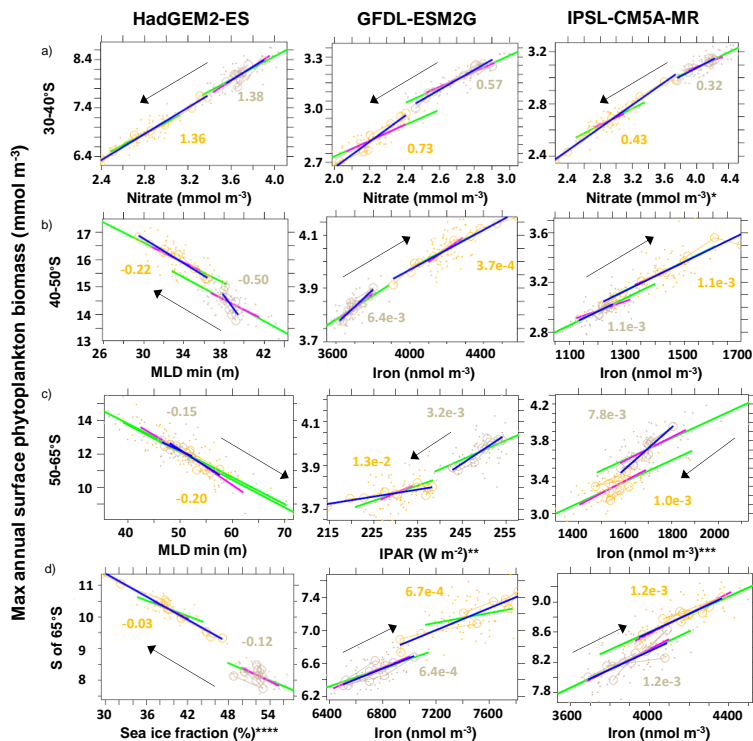


Figure 1. All-model mean 100-year changes in **(a)** maximum annual surface phytoplankton biomass (PB), **(b)** average annual 100 m depth vertically integrated primary production (PP), **(c)** wintertime surface nitrate concentration, **(d)** summertime mixed layer depth (MLD), **(e)** wintertime surface dissolved iron concentration, **(f)** summertime incident photosynthetically available radiation (IPAR), **(g)** summertime percentage area of grid cell covered by clouds, and **(h)** average annual zonal wind stress. Hatched areas are where greater than 80 % of model realizations agree on the sign of the change using a bootstrap significance test (see Sect. 2.4 for methodological details). Zero contours for PP change are plotted over each map. The number of models (n) and the total model weight (w) taken into account for each variable are listed in Fig. S16. Historical all-model mean maps are presented in Figs. S1–9.

[Title Page](#)
[Abstract](#)
[Introduction](#)
[Conclusions](#)
[References](#)
[Tables](#)
[Figures](#)
[Back](#)
[Close](#)
[Full Screen / Esc](#)
[Printer-friendly Version](#)
[Interactive Discussion](#)

A
latitudinally-banded
phytoplankton
response

S. Leung et al.



CONTROL time series (detrended)
(interannual and 5-year mechanisms)

- Yearly data (*historical* 1911-2005)
- Yearly data (*rcp8.5* 2006-2100)
- Best linear fit (yearly data)
- Best linear fit (5-year data)

CLIMATE CHANGE time series (with trend)
(mechanisms driven by climate warming)

- 10-year averages (*historical* 1911-2005)
- 10-year averages (*rcp8.5* 2006-2100)
- Best linear fit (10-year averages)
- ➔ Direction of change with climate warming

Title Page

Abstract

Introduction

Conclusions

References

Tables

Figures

⏪

⏩

◀

▶

Back

Close

Full Screen / Esc

Printer-friendly Version

Interactive Discussion



Figure 2. Drivers of phytoplankton biomass on multiple timescales. Scatter plots of PB vs. the listed variable on interannual and 5-year (both with their climate change signals removed) as well as 10-year timescales. Each column corresponds to a different model, while each row corresponds to a different zonal band. Slopes of the *historical* and *rcp8.5* 10-year average best-fit lines are listed. Only variables with significant ($p < 0.05$) best-fit lines on at least two out of the three timescales studied (interannual, 5-year, and 10-year) are shown. Best-fit lines are drawn only when correlations are significant ($p < 0.05$). Variables tested were wintertime wind stress, MLD and surface iron, nitrate, and silicate concentrations; summertime IPAR, sea surface temperature, and MLD; and average annual surface salinity, zooplankton concentrations, and cloud and sea ice cover. See Sects. 2.5 and 2.6 for further methodological details. *Wintertime MLD was also significant on all three timescales. **Summertime MLD and avg annual cloud cover were also significant on all three timescales. ***Wintertime MLD was also significant on all three timescales. ****The y-axis here is PP ($\mu\text{mol m}^{-2} \text{s}^{-1}$), instead of PB because no variables were significantly correlated on at least two timescales with PB. Summertime IPAR was also significant on the same timescales as average annual sea ice cover.

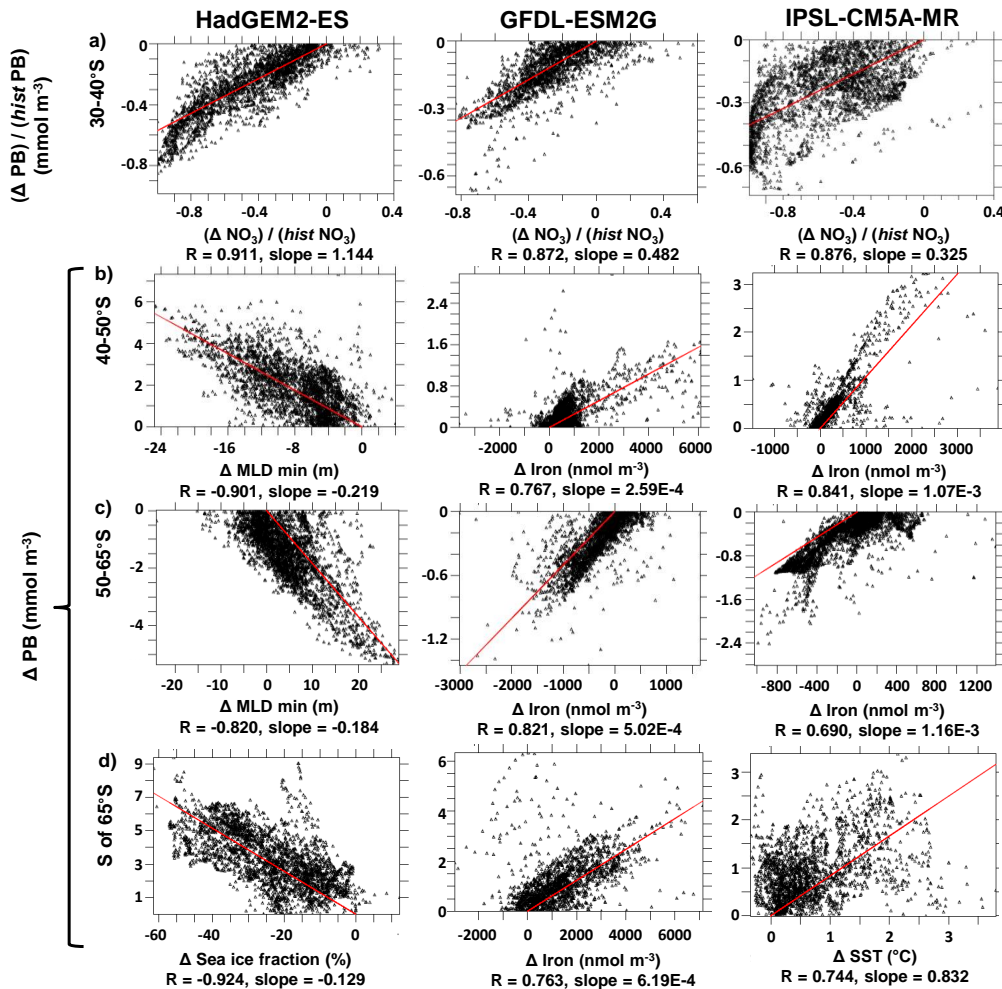
A latitudinally-banded phytoplankton response

S. Leung et al.

[Title Page](#)[Abstract](#)[Introduction](#)[Conclusions](#)[References](#)[Tables](#)[Figures](#)[◀](#)[▶](#)[◀](#)[▶](#)[Back](#)[Close](#)[Full Screen / Esc](#)[Printer-friendly Version](#)[Interactive Discussion](#)

A latitudinally-banded phytoplankton response

S. Leung et al.



Title Page

Abstract Introduction

Conclusions References

Tables Figures

◀ ▶

◀ ▶

Back Close

Full Screen / Esc

Printer-friendly Version

Interactive Discussion



Figure 3. Spatial correlation scatter plots of 100-year changes in phytoplankton biomass vs. 100-year changes in driving variables of interest. Each column corresponds to a different model, while each row corresponds to a different zonal band. Only the variable of interest with the largest magnitude correlation coefficient is plotted for each zone within each model. Variables tested were wintertime wind stress, MLD and surface iron, nitrate, and silicate concentrations; summertime IPAR, sea surface temperature, and MLD; and average annual surface salinity, zooplankton concentrations, and cloud and sea ice cover. Relative changes are plotted for PB vs. nitrate, while absolute changes are plotted for PB vs. all other variables. Best-fit lines are forced to have a zero-intercept. Correlation coefficients and slopes of best-fit lines corresponding to absolute 100-year changes (to facilitate comparison with slopes in Fig. 2) are listed beneath the variable names.

A latitudinally-banded phytoplankton response

S. Leung et al.

[Title Page](#)[Abstract](#)[Introduction](#)[Conclusions](#)[References](#)[Tables](#)[Figures](#)[⏪](#)[⏩](#)[◀](#)[▶](#)[Back](#)[Close](#)[Full Screen / Esc](#)[Printer-friendly Version](#)[Interactive Discussion](#)

A latitudinally-banded phytoplankton response

S. Leung et al.

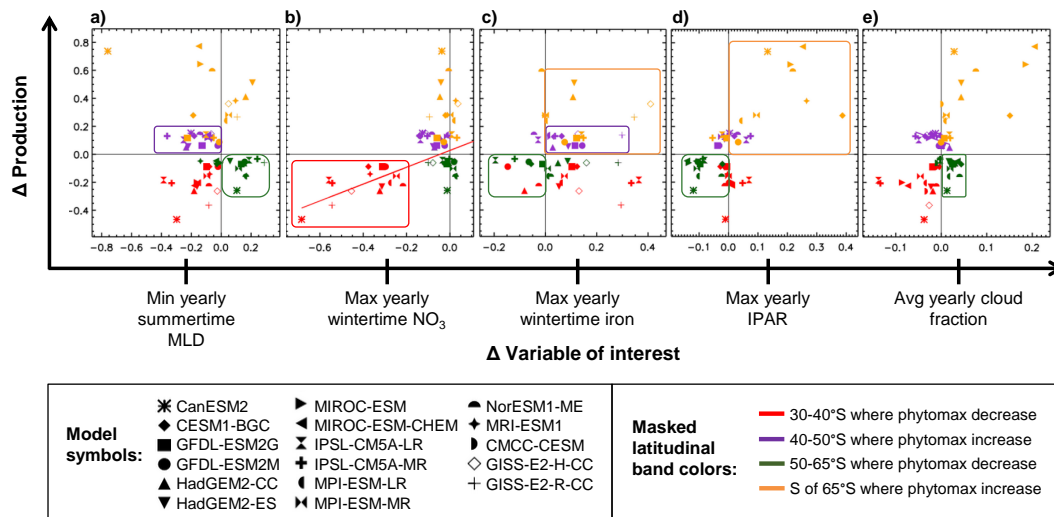


Figure 4. Drivers of 100-year phytoplankton biomass changes across CMIP5 models, by model and latitudinal band. Scatter plots of each model's 100-year relative change in PP vs. its corresponding relative change in the listed variable within each zonal band. Each color represents a different zonal band, while each symbol represents a different model. Colored boxes enclose points which behave in line with our expectations and proposed mechanisms based on Figs. 1–3. Best-fit lines are drawn only when correlations are significant ($p < 0.05$).

Title Page

Abstract

Introduction

Conclusions

References

Tables

Figures

◀

▶

◀

▶

Back

Close

Full Screen / Esc

Printer-friendly Version

Interactive Discussion



A latitudinally-banded phytoplankton response

S. Leung et al.

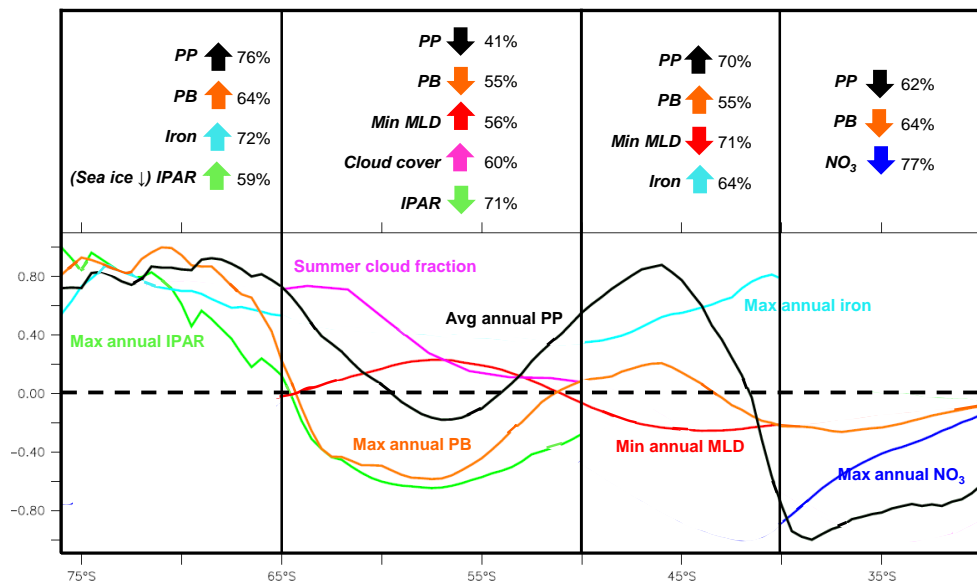


Figure 5. Summary of predicted phytoplankton responses and their drivers within each zonal band, along with normalized 100-year all-model mean zonal changes. Each variable was normalized by first computing the all-model mean zonally-averaged 100-year change at every latitude and then dividing by the absolute value of the largest of these changes occurring south of 30° S. Only the most important driving variables within each band are plotted. Listed above each band is the percentage of model realizations that agree on the sign of the change (based on a bootstrap analysis – see Sect. 2.4 and Fig. S16) in each variable within that band. The number of models (n) and the total model weight (w) taken into account for each variable are listed in Fig. S16.

Title Page

Abstract

Introduction

Conclusions

References

Tables

Figures

◀

▶

◀

▶

Back

Close

Full Screen / Esc

Printer-friendly Version

Interactive Discussion



A latitudinally-banded phytoplankton response

S. Leung et al.

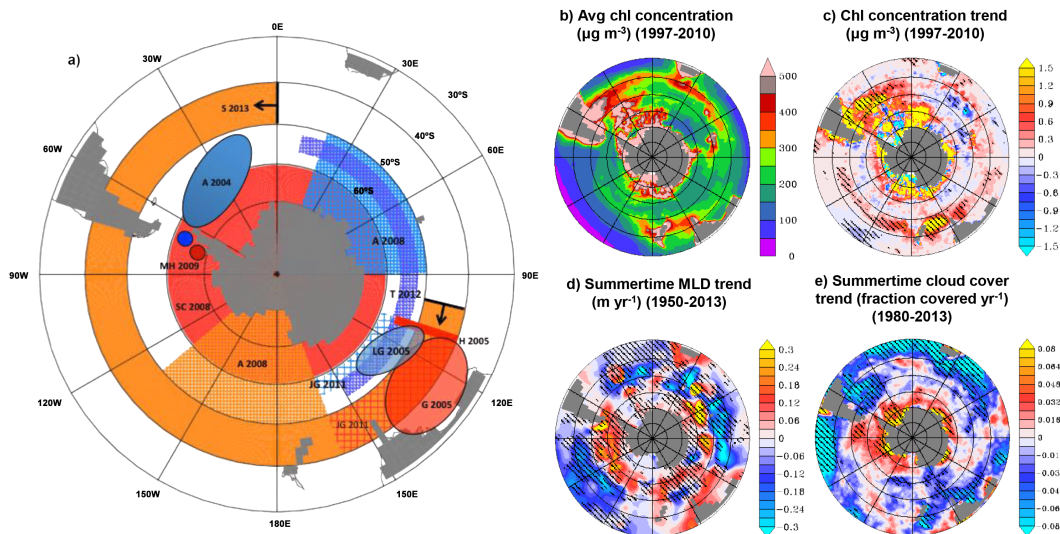


Figure 6. Observed phytoplankton trends and variability. **(a)** Summary of past studies looking at trends and SAM-driven variability in phytoplankton biomass and productivity. Orange/red regions are areas where past studies have found positive trends in phytoplankton biomass or productivity, whereas blue regions are areas where past studies have found negative trends. Each colored region or point is labeled with the corresponding publication. See Table S3 for further details on each study. **(b)** Average observed chl concentrations from SeaWiFS, along with observed trends in **(c)** chl concentrations from SeaWiFS, **(d)** summertime cloud cover from ERA-INTERIM reanalysis, and **(e)** summertime MLD from Hadley reanalysis. Hatched areas are where trends are significant at $p < 0.05$.

Title Page

Abstract

Introduction

Conclusions

References

Tables

Figures

◀

▶

◀

▶

Back

Close

Full Screen / Esc

Printer-friendly Version

Interactive Discussion